

Drell–Yan lepton pair production at low invariant masses: transverse-momentum resummation and non-perturbative effects in QCD

Stefano Camarda^(a), Giancarlo Ferrera^(b) and Lorenzo Rossi^(b)

^(a) CERN, CH-1211 Geneva, Switzerland

^(b) Dipartimento di Fisica, Università di Milano and
INFN, Sezione di Milano, I-20133 Milan, Italy

Abstract

We consider the transverse-momentum (q_T) distribution of Drell-Yan lepton pairs produced with invariant masses (M) from low values up to the Z -boson peak ($4 \leq M \leq 116$ GeV). We present perturbative predictions obtained by consistently combining the resummation of logarithmically enhanced QCD corrections at small q_T ($q_T \ll M$) up to next-to-next-to-next-to-next-to-leading logarithmic accuracy with the available fixed-order calculations at next-to-next-to-leading order (i.e. $\mathcal{O}(\alpha_S^3)$) valid at large q_T . For very low q_T ($q_T \sim \Lambda_{\text{QCD}}$), non-perturbative (NP) QCD effects become dominant and have been included through a NP form factor with a small number of free-parameters. We compare our results with multiple experimental datasets from hadron colliders, finding excellent agreement between theory and data. By fitting the NP parameters, we achieve a precise extraction of the NP form factor and the so-called Collins-Soper kernel.

1 Introduction

The production of Drell–Yan (DY) lepton pairs with high invariant masses ($M \gg \Lambda_{\text{QCD}}$), mediated by a neutral gauge boson (γ^*/Z), is a benchmark process measured with high precision at hadron colliders [1, 2]. It provides important tests of the Standard Model (SM) through precise measurements of its fundamental parameters [3–6] and also imposes constraints on new physics [7]. Thus, accurate theoretical predictions for DY production cross sections and corresponding kinematical distributions are essential. Among these distributions, the transverse momentum (q_T) spectrum of the lepton pair plays a special role. In particular, the q_T spectrum of the Z boson provides key insights into the q_T spectrum of the W boson, whose uncertainty, in turn, directly impacts the measurement of the W boson mass [5, 6, 8–10].

In the region where $q_T \simeq M$, the QCD perturbative series is controlled by a small expansion parameter, $\alpha_S(M^2)$, and the fixed-order expansion in the QCD coupling α_S is theoretically justified. In the intermediate- and low- q_T region, $\Lambda_{\text{QCD}} \ll q_T \ll M$, large logarithmic corrections of infrared origin, of the form $\alpha_S^n/q_T^2 \ln^m(M^2/q_T^2)$ (with $0 \leq m \leq 2n - 1$), spoil the convergence of the fixed-order expansion. In this region, resummation techniques become mandatory. Finally, at very low q_T , $\Lambda_{\text{QCD}} \lesssim q_T$, non-perturbative (NP) effects become dominant and cannot be neglected. However, these regions are in general not well separated in real (experimental) cases. Therefore, to obtain reliable and accurate predictions, it is essential to develop a theoretically consistent formalism capable of describing all the above regions in an unified and consistent framework.

Various different formalisms have been developed with the goal of performing all-order resummation of logarithmically-enhanced terms at small q_T [11–24]. In this paper we follow the general method for transverse-momentum resummation of colorless high mass systems $M \gg \Lambda_{\text{QCD}}$ developed in Refs. [25–27] and applied in the case of Higgs, vector boson and diboson production [28–34]. This formalism has been implemented, in the case of Drell–Yan production, in the `DYTurbo` public numerical program [35, 36] starting from the numerical implementations of Refs. [28, 34].

Phenomenological studies of the q_T spectrum of lepton pairs with an invariant mass (M) of the order of the Z -boson mass $M \sim m_Z$ at the Tevatron and the LHC, using the formalism of Refs. [25–27], have been performed in [28, 37, 38].

In particular, it has been shown in [28], that q_T resummed (and matched) predictions within a purely perturbative approach for the q_T recoil dynamics give a good description, within the perturbative uncertainties, of the experimental data from Tevatron and LHC for $M \sim m_Z$ except at very low q_T values ($q_T \sim 1$ GeV).

In this paper, we extend the analysis of Ref. [28], also considering the region of lower invariant masses $M < m_Z$. This region of invariant masses is more delicate. On the one hand, since the QCD coupling $\alpha_S(M^2)$ increases, higher order corrections become more relevant. On the other hand, approaching the region of very low energies, a breakdown of perturbation theory and the dominance of NP effects is expected [28]. In fact, studies of DY transverse momentum

distributions at low masses with various theoretical approaches and different perturbative accuracy showed contradictory results [39, 40]. Within the present analysis, we confirm the results from Ref. [28], observing that purely perturbative predictions are able to describe, within the errors, experimental data down to $q_T \sim 1$ GeV. Below that region, perturbative predictivity deteriorates and a good description of the data can be obtained only by including NP effects.

NP effects at low q_T can also be incorporated through the formalism of Transverse Momentum Dependent (TMD) Parton Distribution Functions (PDFs), which encode both the longitudinal and transverse momentum distributions of partons inside hadrons. This framework was developed in Refs.[13, 41–43]. The nonperturbative components of TMDs are typically modeled using ansatz functions that depend on several NP parameters to be extracted from the experimental data. For example, the analyses in Refs.[21, 44, 45] employ several tens of free parameters to describe NP effects.

In this paper, we adopt a more minimalistic approach. We incorporate NP effects in the impact-parameter space (i.e., the Fourier conjugate of q_T) by introducing an NP form factor that depends on only four free parameters. Despite its simplicity, this approach provides an excellent description of the experimental data, achieving a fit quality of $\chi^2 \sim 1$ over a wide kinematic range: $4 \leq M \leq 116$ GeV and $0 \leq q_T/M \leq 0.3$.

2 Transverse-momentum resummation and non-perturbative effects

We briefly review the resummation formalism developed in Refs. [26, 28, 34] focussing on the model for NP effects. We consider the process

$$h_1 + h_2 \rightarrow Z/\gamma^* + X \rightarrow l_3 + l_4 + X, \quad (1)$$

where the Z/γ^* boson is produced by the colliding hadrons h_1 and h_2 , while l_3 and l_4 are the final state leptons produced by the decay of the Z/γ^* .

The fully differential hadronic cross section in the lepton kinematics, $d\sigma_{h_1 h_2 \rightarrow l_3 l_4}$ is completely specified by six independent variables. We consider the differential cross section as a function of the two-dimensional transverse-momentum \mathbf{q}_T ($q_T = \sqrt{\mathbf{q}_T^2}$), the rapidity y and the invariant mass M of the lepton pair, and by two generic variables Ω specifying the angular distribution of the leptons with respect to the vector boson momentum. We perform the resummation at the level of partonic cross-section. The differential partonic cross section is decomposed as follows:

$$d\hat{\sigma}_{a_1 a_2 \rightarrow l_3 l_4} = d\hat{\sigma}_{a_1 a_2 \rightarrow l_3 l_4}^{(\text{res.})} + d\hat{\sigma}_{a_1 a_2 \rightarrow l_3 l_4}^{(\text{fin.})} \quad (2)$$

where a_1 and a_2 are the partonic indices and the first term on the right-hand side is the resummed component which contains (and resums) all the logarithmically-enhanced contributions

of the type $\alpha_S^n M^2/q_T^2 \ln^m(M^2/q_T^2)$ (with $0 \leq m \leq 2n - 1$), while the second term is the finite component to be evaluated at fixed order in perturbation theory. More precisely, the finite component is defined in such a way that order-by-order in perturbation theory it fulfills the following equation [26]:

$$\lim_{Q_T \rightarrow 0} \int_0^{Q_T^2} dq_T^2 \left[\frac{d\hat{\sigma}^{(\text{fin.})}}{dq_T^2} \right] = 0. \quad (3)$$

This implies that all the constant terms in b space (corresponding to $\delta(q_T^2)$ terms in q_T space) are included, together with the enhanced logarithms, in $d\hat{\sigma}^{(\text{res.})}$. We evaluate the finite (or remainder) term by subtracting the expansion of the resummed part from the standard fixed-order perturbative expression of the partonic cross section at the same order.

This matching procedure between resummed and fixed-order results (together with the perturbative unitarity constraint we implement on the total cross section) avoids the introduction of large and unjustified higher-order terms at large q_T and allows us to obtain, in such a region, a matched result which is consistent with the fixed-order expansion.

The resummation is performed in the impact-parameter space b (conjugated to q_T) [12] and the resummed component at partonic level is written in the following factorized form [26][†]:

$$d\hat{\sigma}_{a_1 a_2 \rightarrow l_3 l_4}^{(\text{res.})} = \sum_q d\hat{\sigma}_{q\bar{q} \rightarrow l_3 l_4}^{(0)} \mathcal{H}_{a_1 a_2 \rightarrow V}(M, \alpha_S; \mu_R, \mu_F, Q) \times \exp\{\mathcal{G}(\alpha_S, \tilde{L}; \mu_R, Q)\}, \quad (4)$$

where

$$\mathcal{G}(\alpha_S, \tilde{L}) = - \int_{b_0^2/b^2}^{Q^2} \frac{dq^2}{q^2} \left[A(\alpha_S(q^2)) \ln \frac{M^2}{q^2} + B(\alpha_S(q^2)) + 2\beta(\alpha_S(q^2)) \frac{d \ln C(\alpha_S(q^2))}{d \ln \alpha_S(q^2)} + 2\gamma(\alpha_S(q^2)) \right], \quad (5)$$

and we have introduced the logarithmic expansion parameter $\tilde{L} \equiv \ln(Q^2 b^2 / b_0^2 + 1)$ with $b_0 = 2e^{-\gamma_E}$ ($\gamma_E = 0.5772\dots$ is the Euler number). The scales μ_R and μ_F are the customary renormalization and factorization scales, while $Q \sim M$ is the resummation scale whose variations can be used to estimate the effect of uncalculated logarithmic terms at higher orders [46].

The function $A(\alpha_S)$ controls the exponentiation of the double-logarithmic series, while the single logarithms are controlled by the functions $B(\alpha_S)$, $C(\alpha_S)$ and $\gamma(\alpha_S)$. The functions $C(\alpha_S)$ and $\gamma(\alpha_S)$ (which depend on Mellin and flavour indices) are the collinear functions [47] and the moments of the customary Altarelli–Parisi splitting functions.

The functions appearing in Eq. (5) are perturbative series in α_S :

$$A(\alpha_S) = \sum_{n=1}^{\infty} \left(\frac{\alpha_S}{\pi} \right)^n A^{(n)}, \quad B(\alpha_S) = \sum_{n=1}^{\infty} \left(\frac{\alpha_S}{\pi} \right)^n B^{(n)}, \quad (6)$$

$$C(\alpha_S) = \sum_{n=0}^{\infty} \left(\frac{\alpha_S}{\pi} \right)^n C^{(n)}, \quad \gamma(\alpha_S) = \sum_{n=1}^{\infty} \left(\frac{\alpha_S}{\pi} \right)^n \gamma^{(n)}, \quad (7)$$

[†]Resummation of large logarithms is better expressed by working in the Mellin (N -moment) space. For the sake of simplicity we omit the explicit dependence on Mellin indices and on flavour indices.

and $\beta(\alpha_S)$ is the QCD β function:

$$\frac{d \ln \alpha_S(\mu_R^2)}{d \ln \mu_R^2} = \beta(\alpha_S(\mu_R)). \quad (8)$$

The factor $d\hat{\sigma}_{q\bar{q}\rightarrow l_3 l_4}^{(0)}$ in Eq. (4) is the Born level differential cross section for the quark-antiquark annihilation subprocess $q\bar{q} \rightarrow V \rightarrow l_3 l_4$. The functions $\mathcal{H}_{a_1 a_2 \rightarrow V}$ [25, 48–50] are (process dependent) coefficients that contain the hard-collinear contributions and have a standard fixed-order expansion in powers of $\alpha_S = \alpha_S(\mu_R^2)$.

The universal (process independent) form factor $\exp\{\mathcal{G}\}$ contains and resums in an exponentiated form all the $\alpha_S^k \tilde{L}^k$ (with $k \geq 1$) logarithmic terms that order-by-order in α_S are logarithmically divergent as $b \rightarrow \infty$ (i.e. $q_T \rightarrow 0$).

The $N^k\text{LL}+N^k\text{LO}$ accuracy in the small- q_T region means that we include all the logarithmic terms of the type $\alpha_S^n \tilde{L}^{n+1}$ down to $\alpha_S^n \tilde{L}^{n+1-k}$ in the function \mathcal{G} and we evaluate the functions $\mathcal{H}_{a_1 a_2 \rightarrow V}$ up to $N^k\text{LO}$ (i.e. $\mathcal{O}(\alpha_S^k)$). Following Ref. [38] we have reached the $N^4\text{LL}+N^4\text{LO}$ approximated accuracy, where the missing part of the $\mathcal{H}_{a_1 a_2 \rightarrow V}$ coefficients at $\mathcal{O}(\alpha_S^4)$ has been approximated.

We have then consistently matched the resummed results with the fixed-order calculations at high q_T , including finite terms in Eq. (2) up to $\mathcal{O}(\alpha_S^3)$. These contributions are now implemented in the DYTurbo public numerical program [36], following the implementation of Ref. [51], and have been benchmarked against MCFM [51, 52], as well as, upon integration over q_T , against the inclusive cross section computed at the same perturbative order [53].

The function \mathcal{G} is singular when $\alpha_S \tilde{L} = \pi/\beta_0$ (where β_0 is the one-loop coefficient of the QCD β function) which corresponds to the region of transverse-momenta of the order of the Landau pole of the QCD coupling or $b^{-1} \sim \Lambda_{\text{QCD}}$. This signals that a truly non-perturbative region is approached and perturbative results (including resummed ones) are not reliable. In this region, a model for NP QCD effects is required, which must include a regularization of the singular behavior of the function \mathcal{G} . As noted in Refs. [54–57], the specific form of this regularization remains somewhat arbitrary. In this work, we adopt the so-called b_* prescription, originally proposed in Ref. [13], by freezing the b dependence of $\exp G(\alpha_S, \tilde{L})$ before it reaches the Landau singularity.

To achieve this, a parameter b_{max} is introduced with the replacement

$$b \rightarrow b_* = \frac{b}{\sqrt{1 + \frac{b^2}{b_{\text{max}}^2}}}. \quad (9)$$

This prescription guarantees that the variable b_* saturates to b_{max} at large values of b . However, b_* also introduces spurious power corrections that scale like $(\Lambda_{\text{QCD}}/q_T)^k$ [55, 56, 58, 59], with $k > 0$. In the region $q_T \simeq \Lambda_{\text{QCD}}$, these power corrections become sizeable and have to be modelled by including in Eq. (4) a non-perturbative form factor.

We incorporate NP effects through a NP form factor of the form $\exp\{\mathcal{G}_{NP}(b, Q/Q_0)\}$ [28] which multiplies the perturbative form factor $\exp\{\mathcal{G}(\alpha_S, \tilde{L})\}$ appearing in Eq. (4). We adopt a NP form factor inspired by the model proposed in Ref. [60], with the following functional form:

$$\mathcal{G}_{NP}(b, M^2/Q_0^2) = \exp \left[-g_j(b) - g_K(b) \log \frac{M^2}{Q_0^2} \right]. \quad (10)$$

The function $g_j(b)$ accounts for the non-perturbative part of the TMDs, or, more generally, for the intrinsic transverse momentum of the parton inside the parent hadron, at $M = Q_0$. We have used the following parameterization for $g_j(b)$ from Ref. [61]

$$g_j(b) = \frac{g_1 b^2}{1 + \lambda b^2} + \text{sign}(q) \left(1 - \exp[-|q|b^4] \right). \quad (11)$$

We note that we have not included an additional flavour dependence in $g_j(b)$, because we have obtained a good description of the experimental data even without it. We also observe that recent studies [24, 45, 62] have found that Drell–Yan data alone are not sufficient to constrain flavour dependence of such non-perturbative effects.

The function $g_K(b)$, instead, takes into account for the non-perturbative contribution to the Collins–Soper kernel [42, 63], that is, the M^2 dependence of the TMDs (see Sec. 3.1 for further details).

We have chosen to adopt the following parameterization of $g_K(b)$ proposed in Ref. [60]

$$g_K(b) = g_0 \left(1 - \exp \left[- \frac{C_F \alpha_S (\mu_{b_*}^2) b^2}{\pi g_0 b_{max}^2} \right] \right). \quad (12)$$

Such parameterization fulfills the following criteria: it does not affect the perturbative calculation at small b_T , it saturates to a finite value at large b_T , and in the intermediate region it either does not depend or only weakly depends on the choice of b_{max} . This property is particularly important, since b_{max} itself represents a (hyper)parameter that must be carefully controlled in the fit.

3 Numerical results

In the following, we present a comparison between experimental data and theoretical predictions for Z/γ^* production and leptonic decay. The predictions are obtained at central scales, i.e., $\mu_R = \mu_F = Q = M$, and at N⁴LL+N⁴LO[‡] approximated accuracy [38] by matching the resummed calculation with fixed-order results at large q_T , up to NNLO. The hadronic cross section is computed by convoluting the partonic cross section in Eq.(4) with the PDFs from the MSHT set[64] at N³LO, using $\alpha_s(m_Z^2) = 0.118$. For the electroweak couplings, we adopt the so-called G_μ scheme, with the corresponding input parameters listed in Table 1.

[‡]We have checked that the use of N³LL+N³LO accuracy has a very small impact on the results presented.

Constant	Value	Unit
G_F	1.1663787×10^{-5}	GeV^{-2}
m_Z	91.1876	GeV
Γ_Z	2.4950	GeV
m_W	80.385	GeV

Table 1: Numerical values of the electroweak constants used as input for the G_μ scheme in our calculations.

Our calculation includes the leptonic decays $Z/\gamma^* \rightarrow \ell^+\ell^-$, taking into account the effects of Z/γ^* interference and the finite width Γ_Z of the Z boson. Even if the measurements considered in the analysis are inclusive in the lepton kinematics, our calculation can retain spin correlations and the full dependence on the kinematical variables of the final-state leptons.

The datasets considered in our numerical analysis are listed in Tab. 2. Although this is not a global analysis including all available data, it encompasses both high- and low-energy measurements, originating from collider experiments (ATLAS and CDF) and fixed-target experiments (E605 and E288), respectively. The selected data span a broad kinematic range and provide sensitivity to different regions of phase space. Moreover, as shown in the table, the datasets differ in their coverage and structure: some are subject to cuts in rapidity y , others in Feynman- x (x_F) variable, and some are fully inclusive. The selected dataset has been chosen to be sufficiently representative to demonstrate the robustness of our results. In total, we analyze 378 data points. For clarity, we note that in this work we include the majority of the available data points in the q_T spectra for the low invariant mass region, i.e. from fixed-target experiments, and for the high-energy datasets we include data up to $q_T < 30$ GeV. This choice is motivated by our primary interest in describing the low invariant mass region, together with the fact that the applicability of the this formalism to high-energy data has already been extensively validated in the literature.

To determine the optimal values of the nonperturbative parameters entering Eqs. (10)-(12), we performed a fit by interfacing `DYTurbo` with `xFitter` [69]. In particular, the best-fit parameters were obtained by minimizing a χ^2 function that accounts for both experimental and theoretical uncertainties, the latter arising from PDF variations. The χ^2 function is defined as

$$\chi^2(\beta_{\text{exp}}, \beta_{\text{th}}) = \sum_{i=1}^{N_{\text{dat}}} \frac{\left(\sigma_i^{\text{exp}} + \sum_j \Gamma_{ij}^{\text{exp}} \beta_{j,\text{exp}} - \sigma_i^{\text{th}} - \sum_k \Gamma_{ik}^{\text{th}} \beta_{k,\text{th}} \right)^2}{\Delta_i^2} + \sum_j \beta_{j,\text{exp}}^2 + \sum_k \beta_{k,\text{th}}^2, \quad (13)$$

where the index i runs over all N_{dat} data points, while j and k run over the nuisance parameter vectors β_{exp} and β_{th} , which encode the correlated experimental and theoretical (PDF-related) uncertainties, respectively. The effect of each of them on the experimental data and theoretical prediction is described by the response matrices Γ_{ij}^{exp} and Γ_{ik}^{th} . The measurements and the uncorrelated experimental uncertainties are denoted by σ_i^{exp} and Δ_i , respectively, while the theoretical predictions are denoted by σ_i^{th} .

As part of the fitting procedure, we also investigated the dependence of the results on

Experiment	N_{dat}	Observable	\sqrt{s} [GeV]	Q [GeV]	y or x_F	Ref.
E605	74	$Ed^3\sigma/d^3\mathbf{q}$	38.8	7 - 18	$x_F = 0.1$	[65]
E288 200 GeV	50	$Ed^3\sigma/d^3\mathbf{q}$	19.4	4 - 9	$y = 0.40$	[66]
E288 300 GeV	59	$Ed^3\sigma/d^3\mathbf{q}$	23.8	4 - 12	$y = 0.21$	[66]
E288 400 GeV	68	$Ed^3\sigma/d^3\mathbf{q}$	27.4	5 - 14	$y = 0.03$	[66]
CDF Run II	55	$d\sigma/dq_T$	1960	66 - 116	Inclusive	[67]
ATLAS 8 TeV	9	$(1/\sigma)d\sigma/dq_T$	8000	80 - 100	$0 < y < 0.4$	[68]
	9				$0.4 < y < 0.8$	
	9				$0.8 < y < 1.2$	
	9				$1.2 < y < 1.6$	
	9				$1.6 < y < 2.0$	
	9				$2.0 < y < 2.4$	
	9				$2.4 < y < 2.8$	
9	$2.8 < y < 3.6$					
Total	378					

Table 2: Experimental data sets included in this analysis. Each row contains the number of data points (N_{dat}), the measured observable, the center-of-mass energy \sqrt{s} , the invariant mass range, the acceptance region in the variable y or x_F , and the published reference.

the parameters Q_0 and b_{max} appearing in Eqs. (9)–(12), which are typically chosen a priori. We found that the quality of the fit, as reflected in the predictions and quantified by the resulting χ^2 , is largely insensitive to variations in these parameters[§]. Nevertheless, in order to fix their values, we identified the most stable and accurate configuration as $Q_0 = 1$ GeV and $b_{\text{max}} = 1.5$ GeV⁻¹. The final fit yields a reduced chi-squared of $\chi^2/N_{\text{d.o.f.}} = 1.25$, and the corresponding best-fit parameters, along with their uncertainties extracted via the Hessian method, are listed in Tab. 3. The associated covariance matrix is shown in Fig. 1.

	g_0	g_1	λ	q
NP Parameters	0.83 ± 0.14	0.732 ± 0.046	0.92 ± 0.20	-0.136 ± 0.010

Table 3: Values obtained for the free parameters in the fit. For each parameter, the best-fit value and the associated standard deviation are reported.

As we can see from the table, all parameters are reasonably well constrained, although some exhibit significant mutual correlations. Together with the value $\chi^2/N_{\text{d.o.f.}} = 1.25$ [¶], this suggests that the chosen functional form for the non-perturbative component, which involves only a small number of parameters, is capable of providing a good description of the data. The presence of strong correlations is a common feature in fits of hadronic distributions and may indicate that an alternative functional form could improve the description. However, a

[§]This behavior was already suggested in Ref.[13], and we have explicitly confirmed it in our analysis.

[¶]We performed an additional fit using the NNPDF40an3lo Hessian set [70], keeping the same configuration as before, and obtained a $\chi^2/N_{\text{d.o.f.}} = 1.38$. The deterioration in the fit quality is likely due to the smaller PDF uncertainties associated with this set.

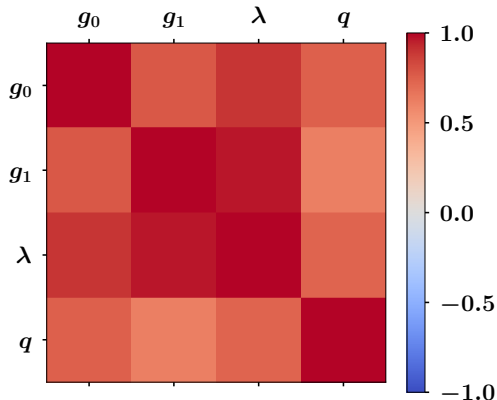


Figure 1: Graphical representation of the correlation matrix for the free parameters of fit.

systematic exploration of this possibility lies beyond the scope of the present work and is left for future studies.

Before presenting the comparison between the data and the predictions obtained from the fit, we emphasize that we performed several fits by varying the set of included data points, particularly by applying different cuts on the ratio $\frac{q_T}{Q}$. We observed that including a larger number of data points generally leads to tighter constraints on the non-perturbative parameters, especially λ and q . In particular, for the fit performed with the cut $\frac{q_T}{Q} \leq 0.2$, which includes 240 data points and corresponds to the typical kinematic range considered in standard TMD fits [21, 44, 44, 45, 62, 71], we obtain a reduced chi-squared of $\chi^2/N_{\text{d.o.f.}} = 1.03$. This result is comparable to, or even better than, those from existing TMD fits, despite relying on a significantly smaller number of non-perturbative parameters. The quality of the description slightly worsens when data at higher q_T are included, which may be attributed either to statistical issues in the low-energy data or to missing-mass effects and higher-order corrections in the fixed-order contributions, which become more relevant at low invariant masses.

In Fig. 2, we compare the predictions obtained from the fit with the experimental data from the E605 experiment for the invariant mass bins $7 < M < 8$ GeV and $11.5 < M < 13.5$ GeV. The orange bands represent the PDF uncertainty from the MSHT20an3lo set. As shown, the experimental data are well described within uncertainties across the entire transverse momentum spectrum. This provides clear evidence that the formalism described by Eq. (2), supplemented by a simple non-perturbative model, is capable of accurately describing low invariant mass Drell–Yan data.

Continuing the analysis, Figs. 3 and 4 show the comparison between theoretical predictions and data from the E288 experiment for the invariant mass bins $5 < M < 6$ GeV and $6 < M < 7$ GeV, respectively, at three different beam energies: $E_{\text{beam}} = 200, 300,$ and 400 GeV. In all cases, we observe very good agreement within the combined experimental and theoretical uncertainties. A slight deterioration in the description is observed in the highest q_T bins, which may indicate the presence of missing higher-order corrections or target mass effects, both of

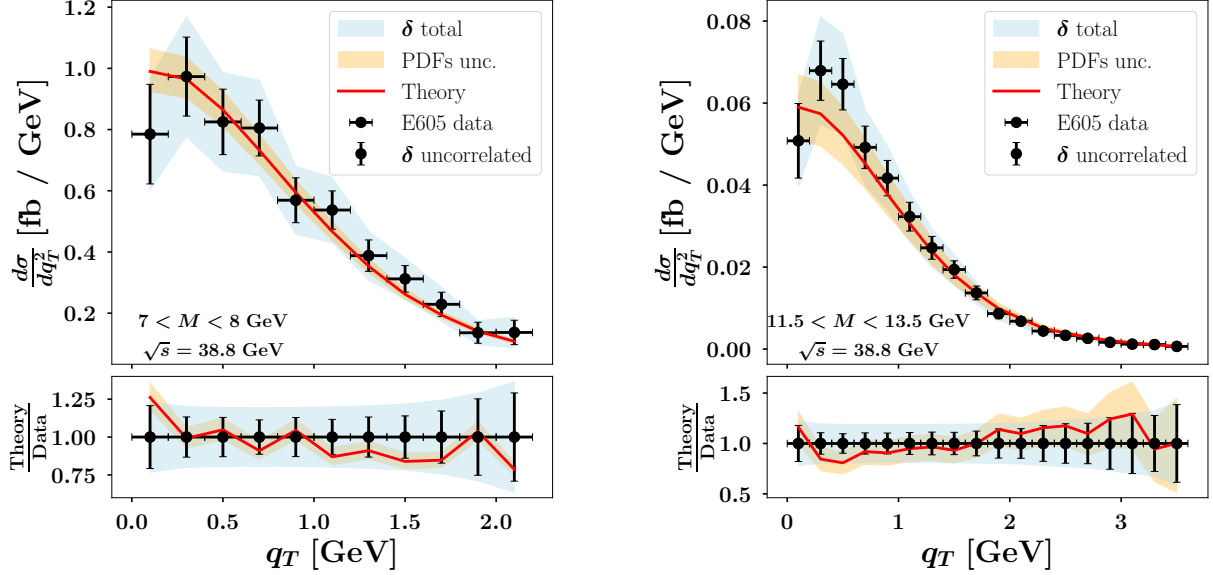


Figure 2: Comparison between theoretical predictions and experimental data for the Drell–Yan cross section differential in q_T from the E605 experiment. The left and right panels correspond to the invariant mass bins $7 < M < 8$ GeV and $11.5 < M < 13.5$ GeV, respectively. The orange bands represent the PDF uncertainty from the MSHT20an3lo set.

which are neglected in the present analysis.

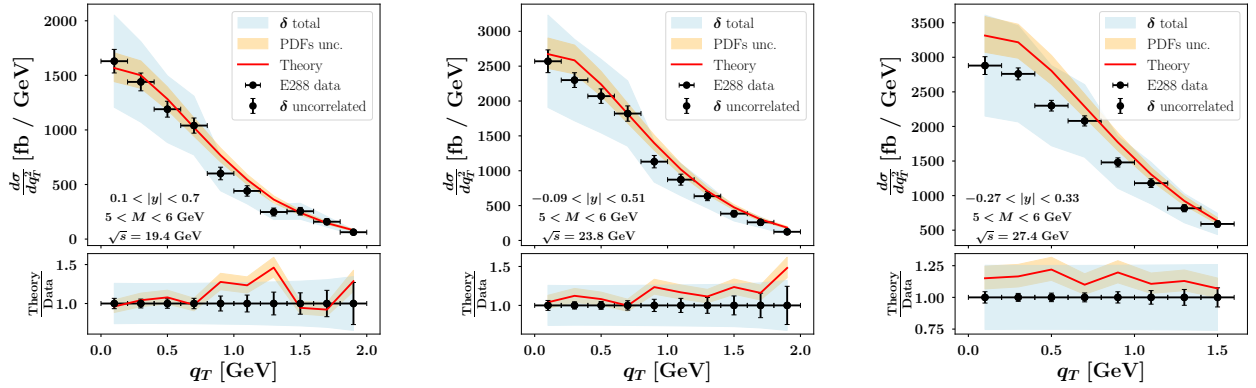


Figure 3: Comparison between theoretical predictions and experimental data for the Drell–Yan cross section differential in q_T from the E288 experiment, in the invariant mass bin $5 < M < 6$ GeV. The left, center, and right panels correspond to beam energies of $E_{\text{beam}} = 200$ GeV, 300 GeV, and 400 GeV, respectively. The orange bands represent the PDF uncertainty from the MSHT20an3lo set.

For completeness, in Fig. 5 we also show the comparison between theoretical predictions and high-energy Drell–Yan data at the Z -boson peak. It is well established in the literature

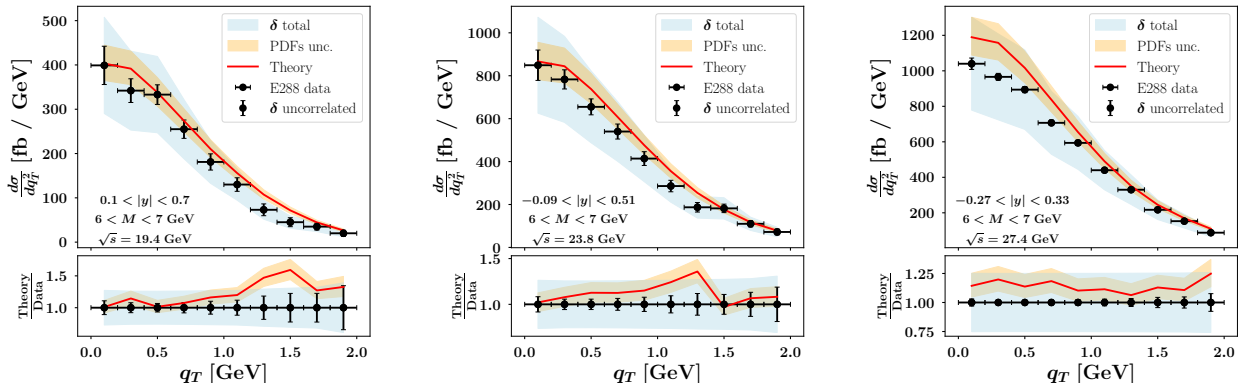


Figure 4: Comparison between theoretical predictions and experimental data for the Drell–Yan cross section differential in q_T from the E288 experiment, in the invariant mass bin $6 < M < 7$ GeV. The left, center, and right panels correspond to beam energies of $E_{\text{beam}} = 200$ GeV, 300 GeV, and 400 GeV, respectively. The orange bands represent the PDF uncertainty from the MSHT20an3lo set.

that these data are accurately described by perturbative QCD combined with a simple non-perturbative model; see, for instance, Refs.[28]. The left panel shows the result for the CDF experiment, while the right panel corresponds to the ATLAS measurement at $\sqrt{s} = 8$ TeV in the central rapidity region $|y| < 0.4$. We observe excellent agreement with the experimental data within the uncertainty bands. Importantly, we find that the same theoretical framework and non-perturbative model used for the low-energy data also provides a consistent and accurate description of the high-energy regime. This confirms the robustness and flexibility of our approach in describing the full range of available Drell–Yan data across different energies.

3.1 Determination of the Collins-Soper Kernel

In recent years, the Collins–Soper kernel has attracted considerable attention, as it plays a crucial role in the TMD formalism by governing the evolution of TMDs with respect to the rapidity scale ζ [42, 63, 72]. Its relevance is further underscored by the fact that it can be directly extracted from experimental data [21, 44, 45, 62, 71] or estimated using lattice QCD calculations [73–78].

The Collins–Soper kernel is related to the cusp anomalous dimension by the following equation [13]

$$\frac{dK(b^2Q^2, \alpha_S(Q^2))}{d \ln Q^2} = -\gamma_K(\alpha_S(Q^2)), \quad (14)$$

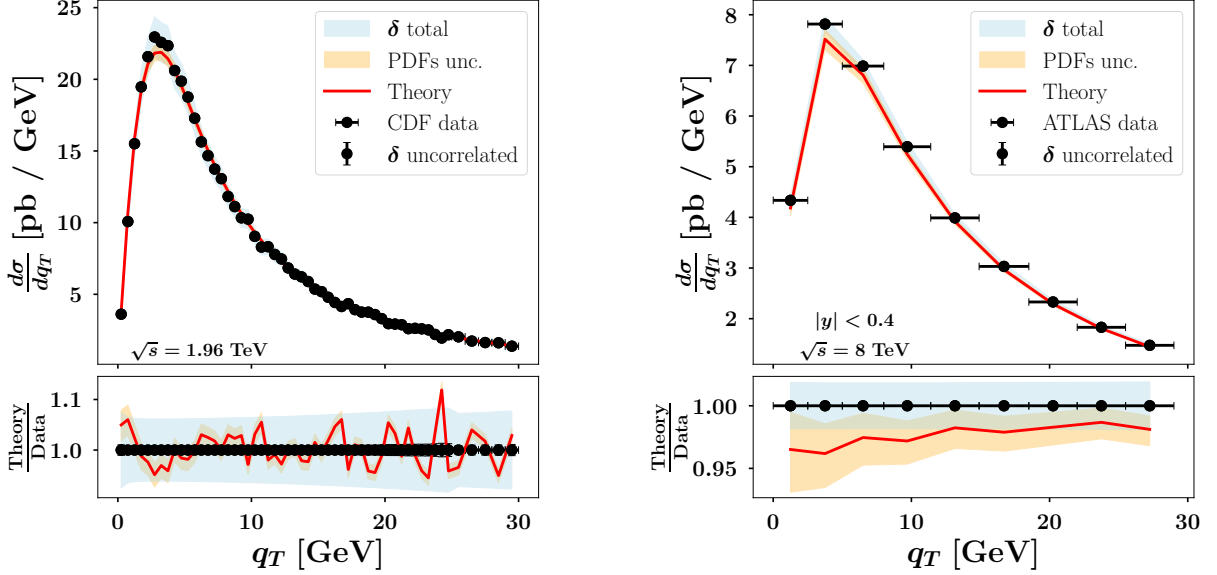


Figure 5: Comparison between theoretical predictions and high-energy Drell–Yan data at the Z -boson peak. The left panel corresponds to the CDF measurement, while the right panel shows the ATLAS data at $\sqrt{s} = 8$ TeV in the central rapidity region $|y| < 0.4$.

where $\gamma_K(\alpha_S)$ is the cusp anomalous dimension. The solution of the above reads

$$K(b^2 Q^2, \alpha_S(Q^2)) = K(b_0^2, \alpha_S(b_0^2/b^2)) - \int_{b_0^2/b^2}^{Q^2} \frac{dq^2}{q^2} \gamma_K(\alpha_S(q^2)). \quad (15)$$

The kernel can be perturbatively expanded as

$$K(b^2 Q^2, \alpha_S) = \sum_{n=1}^{\infty} \left(\frac{\alpha_S}{\pi} \right)^n K^{(n)}(b^2 Q^2). \quad (16)$$

The Collins–Soper kernel can be related to the functions $A(\alpha_S)$ and $B(\alpha_S)$ in Eq. (5), through the relations [13]:

$$A(\alpha_S) = \frac{1}{2} \gamma_K(\alpha_S) + \frac{1}{2} \beta(\alpha_S) \frac{\partial K(b_0^2, \alpha_S)}{\partial \ln \alpha_S}, \quad (17)$$

$$B(\alpha_S) = -\gamma_F(\alpha_S) - K(b_0^2, \alpha_S), \quad (18)$$

and by inverting these relations one can obtain the correspondence between the perturbative coefficients $K^{(n)}$, $\gamma_K^{(n)}$ and $A^{(n)}$, $B^{(n)}$, $\gamma_F^{(n)}$, which arise respectively from the perturbative expansions of the $A(\alpha_S)$ and $B(\alpha_S)$ functions and from the non-cusp anomalous dimension $\gamma_F(\alpha_S)$ ^{||}.

^{||}In Ref. [13], $\gamma_F(\alpha_S)$ was called $G(\alpha_S)$.

The non-perturbative contribution of the Collins–Soper kernel is encoded in the function $g_K(b)$ in Eq. (12).

In Fig. 6 we show the perturbative and non-perturbative contribution to the Collins–Soper kernel as a function of b :

$$K(b, Q) = K(b_*^2 Q^2, \alpha_S) + g_K(b). \quad (19)$$

with the scale fixed, as conventionally in the literature, at $Q = 2$ GeV. The purple uncertainty band accounts for the combined effect of the uncertainty on the fitted parameter g_0 , as well as the variations of b_{\max} in the range 1–2.5 GeV⁻¹ and Q_0 in the range 1–3 GeV. For comparison, the blue dot-dashed lines indicate the uncertainty due to g_0 only. Notably, it also accounts for the uncertainties associated with the choice of b_{\max} , which is often fixed a priori in other analyses, which potentially introduces a theoretical bias.

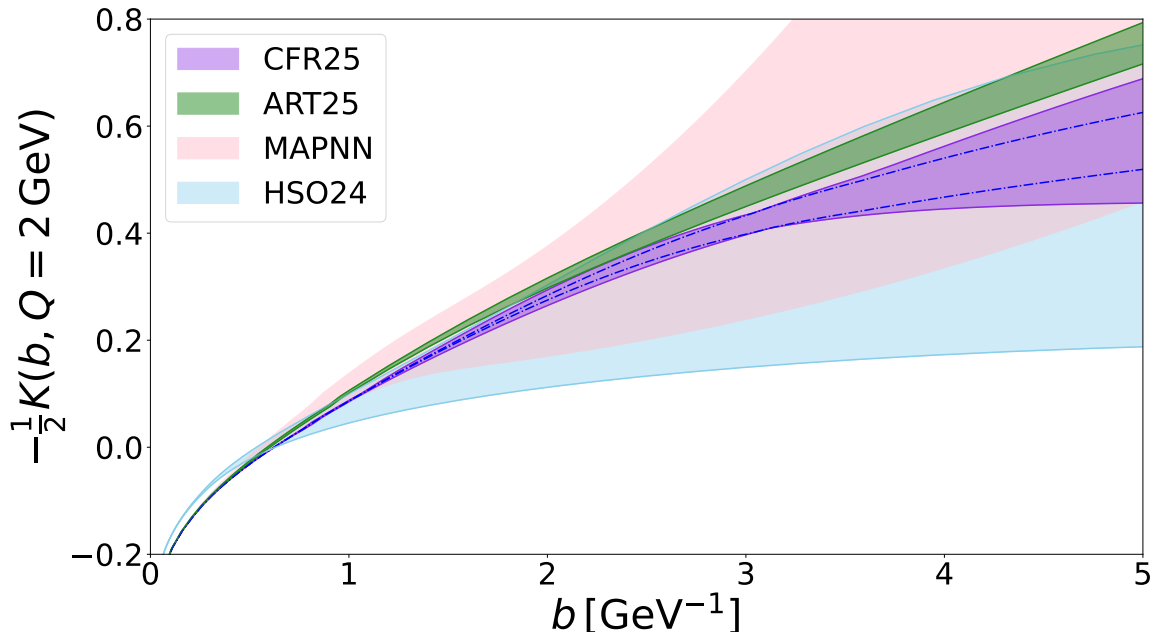


Figure 6: The Collins–Soper kernel as a function of b at the scale $\mu_R = Q = 2$ GeV, as extracted in the present analysis (CFR25), compared to other determinations MAPNN [21], ART25 [44], HSO24 [79]. The purple band represents the combined uncertainties from the parameters g_0 , b_{\max} , and Q_0 , while the blue dot-dashed lines indicate the uncertainty due to g_0 only.

In Fig. 6, we also show a comparison of our extraction of the Collins–Soper kernel against the ones of other groups. Our result is found to be compatible with the latest determination by the MAP Collaboration, obtained from fits to low-transverse-momentum Drell–Yan data [21], as well as with the extraction of Ref. [79], where low-invariant-mass Drell–Yan data were analyzed. It is also in reasonable agreement with the most recent extraction by the ART Collaboration, which is based on combined low-transverse-momentum Drell–Yan and SIDIS data [44]. A slight tension between the uncertainty bands can be observed in this case; however, we note that the authors of Ref. [44] explicitly acknowledge in Ref. [80] that their uncertainty estimates may be somewhat underestimated.

As discussed in the previous section, a more accurate determination of the nonperturbative parameters is obtained when including higher values of q_T than those typically used in TMD fits. Therefore, the most reliable extractions of the Collins–Soper kernel should rely on global analyses that incorporate all available experimental data and exploit the full region in which resummation effects have a non-negligible impact, as emphasized in the present study. A more detailed and dedicated investigation of the Collins–Soper kernel along these lines is left for future work.

4 Conclusions

In this work, we have presented a comprehensive phenomenological analysis of the Drell–Yan transverse-momentum (q_T) distribution, covering a broad kinematic range from low invariant masses up to the Z -boson peak ($4 \leq M \leq 116$ GeV). Our predictions include the state-of-the-art ingredients in perturbative QCD: we combine the resummation of large Sudakov logarithms at N⁴LL accuracy with N⁴LO hard-virtual contributions at small q_T and we consistently match resummed results with the known $\mathcal{O}(\alpha_S^3)$ fixed-order calculation valid at large q_T .

These contributions have been implemented in the `DYTurbo` public numerical program [36] which allows the user to apply arbitrary kinematical cuts on the vector boson and the final-state leptons, and which provides fast and numerically precise predictions for the relevant kinematical distributions.

We have found that, within our resummation formalism of Refs. [25–27], pure perturbative QCD predictions are able to describe, within the errors, experimental data down to $q_T \sim 1$ GeV. At very low values of q_T ($q_T \sim 1$ GeV) non-perturbative (NP) QCD effects are essential and have been included through a NP form factor depending on very few free parameters.

We performed a detailed comparison of our predictions with a wide array of experimental data from fixed-target and collider experiments. We find excellent agreement between our theoretical framework and the data across all energies and q_T ranges analyzed.

The remarkable consistency between theory and data has enabled a precise extraction of the parameters governing the NP form factor and the so-called Collins–Soper kernel.

Acknowledgments. The work of L.R. is partially supported by the Italian Ministero dell’Università e Ricerca (MUR) through the research grant 20229KEFAM (PRIN2022, Next Generation EU, CUP H53D23000980006).

References

- [1] S. Holmes, R. S. Moore and V. Shiltsev, *Overview of the Tevatron Collider Complex: Goals, Operations and Performance*, *JINST* **6** (2011) T08001, [1106.0909].
- [2] *LHC Machine*, *JINST* **3** (2008) S08001.
- [3] S. Camarda, J. Cuth and M. Schott, *Determination of the muonic branching ratio of the W boson and its total width via cross-section measurements at the Tevatron and LHC*, *Eur. Phys. J. C* **76** (2016) 613, [1607.05084].
- [4] CMS collaboration, S. Chatrchyan et al., *Measurement of the weak mixing angle with the Drell-Yan process in proton-proton collisions at the LHC*, *Phys. Rev. D* **84** (2011) 112002, [1110.2682].
- [5] ATLAS collaboration, M. Aaboud et al., *Measurement of the W -boson mass in pp collisions at $\sqrt{s} = 7$ TeV with the ATLAS detector*, *Eur. Phys. J. C* **78** (2018) 110, [1701.07240].
- [6] CDF collaboration, T. Aaltonen et al., *High-precision measurement of the W boson mass with the CDF II detector*, *Science* **376** (2022) 170–176.
- [7] X. Cid Vidal et al., *Report from Working Group 3: Beyond the Standard Model physics at the HL-LHC and HE-LHC*, *CERN Yellow Rep. Monogr.* **7** (2019) 585–865, [1812.07831].
- [8] L. Rottoli, P. Torrielli and A. Vicini, *Determination of the W -boson mass at hadron colliders*, *Eur. Phys. J. C* **83** (2023) 948, [2301.04059].
- [9] CDF, D0 collaboration, T. A. Aaltonen et al., *Combination of CDF and D0 W -Boson Mass Measurements*, *Phys. Rev. D* **88** (2013) 052018, [1307.7627].
- [10] LHCb collaboration, R. Aaij et al., *Measurement of the W boson mass*, *JHEP* **01** (2022) 036, [2109.01113].
- [11] Y. L. Dokshitzer, D. Diakonov and S. I. Troian, *On the Transverse Momentum Distribution of Massive Lepton Pairs*, *Phys. Lett. B* **79** (1978) 269–272.
- [12] G. Parisi and R. Petronzio, *Small Transverse Momentum Distributions in Hard Processes*, *Nucl. Phys. B* **154** (1979) 427–440.
- [13] J. C. Collins, D. E. Soper and G. F. Sterman, *Transverse Momentum Distribution in Drell-Yan Pair and W and Z Boson Production*, *Nucl. Phys. B* **250** (1985) 199–224.
- [14] S. Catani and M. Grazzini, *QCD transverse-momentum resummation in gluon fusion processes*, *Nucl. Phys. B* **845** (2011) 297–323, [1011.3918].
- [15] T. Becher and M. Neubert, *Drell-Yan Production at Small q_T , Transverse Parton Distributions and the Collinear Anomaly*, *Eur. Phys. J. C* **71** (2011) 1665, [1007.4005].

- [16] M. A. Ebert and F. J. Tackmann, *Resummation of Transverse Momentum Distributions in Distribution Space*, *JHEP* **02** (2017) 110, [1611.08610].
- [17] I. Scimemi and A. Vladimirov, *Analysis of vector boson production within TMD factorization*, *Eur. Phys. J. C* **78** (2018) 89, [1706.01473].
- [18] W. Bizoń, X. Chen, A. Gehrmann-De Ridder, T. Gehrmann, N. Glover, A. Huss et al., *Fiducial distributions in Higgs and Drell-Yan production at $N^3LL+NNLO$* , *JHEP* **12** (2018) 132, [1805.05916].
- [19] W. Bizon, A. Gehrmann-De Ridder, T. Gehrmann, N. Glover, A. Huss, P. F. Monni et al., *The transverse momentum spectrum of weak gauge bosons at $N^3LL + NNLO$* , *Eur. Phys. J. C* **79** (2019) 868, [1905.05171].
- [20] T. Becher and M. Hager, *Event-Based Transverse Momentum Resummation*, *Eur. Phys. J. C* **79** (2019) 665, [1904.08325].
- [21] MAP (MULTI-DIMENSIONAL ANALYSES OF PARTONIC DISTRIBUTIONS) collaboration, A. Bacchetta, V. Bertone, C. Bissolotti, M. Cerutti, M. Radici, S. Rodini et al., *Neural-Network Extraction of Unpolarized Transverse-Momentum-Dependent Distributions*, *Phys. Rev. Lett.* **135** (2025) 021904, [2502.04166].
- [22] S. Alioli, C. W. Bauer, A. Broggio, A. Gavardi, S. Kallweit, M. A. Lim et al., *Matching NNLO predictions to parton showers using $N3LL$ color-singlet transverse momentum resummation in geneva*, *Phys. Rev. D* **104** (2021) 094020, [2102.08390].
- [23] M. A. Ebert, J. K. L. Michel, I. W. Stewart and F. J. Tackmann, *Drell-Yan q_T resummation of fiducial power corrections at N^3LL* , *JHEP* **04** (2021) 102, [2006.11382].
- [24] G. Billis, J. K. L. Michel and F. J. Tackmann, *Drell-Yan transverse-momentum spectra at N^3LL' and approximate N^4LL with SCETlib*, *JHEP* **02** (2025) 170, [2411.16004].
- [25] S. Catani, D. de Florian and M. Grazzini, *Universality of nonleading logarithmic contributions in transverse momentum distributions*, *Nucl. Phys. B* **596** (2001) 299–312, [hep-ph/0008184].
- [26] G. Bozzi, S. Catani, D. de Florian and M. Grazzini, *Transverse-momentum resummation and the spectrum of the Higgs boson at the LHC*, *Nucl. Phys. B* **737** (2006) 73–120, [hep-ph/0508068].
- [27] G. Bozzi, S. Catani, D. de Florian and M. Grazzini, *Higgs boson production at the LHC: Transverse-momentum resummation and rapidity dependence*, *Nucl. Phys. B* **791** (2008) 1–19, [0705.3887].
- [28] S. Catani, D. de Florian, G. Ferrera and M. Grazzini, *Vector boson production at hadron colliders: transverse-momentum resummation and leptonic decay*, *JHEP* **12** (2015) 047, [1507.06937].

- [29] S. Catani, L. Cieri, D. de Florian, G. Ferrera and M. Grazzini, *Diphoton production at the LHC: a QCD study up to NNLO*, *JHEP* **04** (2018) 142, [1802.02095].
- [30] L. Cieri, F. Coradeschi and D. de Florian, *Diphoton production at hadron colliders: transverse-momentum resummation at next-to-next-to-leading logarithmic accuracy*, *JHEP* **06** (2015) 185, [1505.03162].
- [31] M. Grazzini, S. Kallweit, D. Rathlev and M. Wiesemann, *Transverse-momentum resummation for vector-boson pair production at NNLL+NNLO*, *JHEP* **08** (2015) 154, [1507.02565].
- [32] D. de Florian, G. Ferrera, M. Grazzini and D. Tommasini, *Transverse-momentum resummation: Higgs boson production at the Tevatron and the LHC*, *JHEP* **11** (2011) 064, [1109.2109].
- [33] D. de Florian, G. Ferrera, M. Grazzini and D. Tommasini, *Higgs boson production at the LHC: transverse momentum resummation effects in the $H \rightarrow 2\gamma$, $H \rightarrow WW \rightarrow l\nu l\nu$ and $H \rightarrow ZZ \rightarrow 4l$ decay modes*, *JHEP* **06** (2012) 132, [1203.6321].
- [34] G. Bozzi, S. Catani, G. Ferrera, D. de Florian and M. Grazzini, *Production of Drell-Yan lepton pairs in hadron collisions: Transverse-momentum resummation at next-to-next-to-leading logarithmic accuracy*, *Phys. Lett. B* **696** (2011) 207–213, [1007.2351].
- [35] S. Camarda et al., *DYTurbo: Fast predictions for Drell-Yan processes*, *Eur. Phys. J. C* **80** (2020) 251, [1910.07049].
- [36] S. Camarda et al. <https://dyturbo.hepforge.org>.
- [37] S. Camarda, L. Cieri and G. Ferrera, *Drell-Yan lepton-pair production: qT resummation at N^3LL accuracy and fiducial cross sections at N^3LO* , *Phys. Rev. D* **104** (2021) L111503, [2103.04974].
- [38] S. Camarda, L. Cieri and G. Ferrera, *Drell-Yan lepton-pair production: qT resummation at N^4LL accuracy*, *Phys. Lett. B* **845** (2023) 138125, [2303.12781].
- [39] A. Bacchetta, G. Bozzi, M. Lambertsen, F. Piacenza, J. Steiglechner and W. Vogelsang, *Difficulties in the description of Drell-Yan processes at moderate invariant mass and high transverse momentum*, *Phys. Rev. D* **100** (2019) 014018, [1901.06916].
- [40] R. Gauld, A. Gehrmann-De Ridder, T. Gehrmann, E. W. N. Glover, A. Huss, I. Majer et al., *Transverse momentum distributions in low-mass Drell-Yan lepton pair production at NNLO QCD*, *Phys. Lett. B* **829** (2022) 137111, [2110.15839].
- [41] J. C. Collins, D. E. Soper and G. F. Sterman, *Factorization of Hard Processes in QCD*, *Adv. Ser. Direct. High Energy Phys.* **5** (1989) 1–91, [hep-ph/0409313].
- [42] J. C. Collins and D. E. Soper, *Back-To-Back Jets in QCD*, *Nucl. Phys. B* **193** (1981) 381.

- [43] J. C. Collins, D. E. Soper and G. F. Sterman, *Factorization for Short Distance Hadron - Hadron Scattering*, *Nucl. Phys. B* **261** (1985) 104–142.
- [44] V. Moos, I. Scimemi, A. Vladimirov and P. Zurita, *Determination of unpolarized TMD distributions from the fit of Drell-Yan and SIDIS data at N^4LL* , 2503.11201.
- [45] MAP (MULTI-DIMENSIONAL ANALYSES OF PARTONIC DISTRIBUTIONS) collaboration, A. Bacchetta, V. Bertone, C. Bissoletti, G. Bozzi, M. Cerutti, F. Delcarro et al., *Flavor dependence of unpolarized quark transverse momentum distributions from a global fit*, *JHEP* **08** (2024) 232, [2405.13833].
- [46] G. Bozzi, S. Catani, D. de Florian and M. Grazzini, *The $q(T)$ spectrum of the Higgs boson at the LHC in QCD perturbation theory*, *Phys. Lett. B* **564** (2003) 65–72, [hep-ph/0302104].
- [47] S. Catani and P. K. Dhani, *Collinear functions for QCD resummations*, *JHEP* **03** (2023) 200, [2208.05840].
- [48] S. Catani, L. Cieri, D. de Florian, G. Ferrera and M. Grazzini, *Universality of transverse-momentum resummation and hard factors at the NNLO*, *Nucl. Phys. B* **881** (2014) 414–443, [1311.1654].
- [49] S. Catani, L. Cieri, D. de Florian, G. Ferrera and M. Grazzini, *Vector boson production at hadron colliders: hard-collinear coefficients at the NNLO*, *Eur. Phys. J. C* **72** (2012) 2195, [1209.0158].
- [50] T. Gehrmann, T. Lubbert and L. L. Yang, *Transverse parton distribution functions at next-to-next-to-leading order: the quark-to-quark case*, *Phys. Rev. Lett.* **109** (2012) 242003, [1209.0682].
- [51] T. Neumann and J. Campbell, *Fiducial Drell-Yan production at the LHC improved by transverse-momentum resummation at N_4LLp+N_3LO* , *Phys. Rev. D* **107** (2023) L011506, [2207.07056].
- [52] R. Boughezal, J. M. Campbell, R. K. Ellis, C. Focke, W. T. Giele, X. Liu et al., *Z-boson production in association with a jet at next-to-next-to-leading order in perturbative QCD*, *Phys. Rev. Lett.* **116** (2016) 152001, [1512.01291].
- [53] J. Baglio, C. Duhr, B. Mistlberger and R. Szafron, *Inclusive production cross sections at N^3LO* , *JHEP* **12** (2022) 066, [2209.06138].
- [54] J.-w. Qiu and X.-f. Zhang, *Role of the nonperturbative input in QCD resummed Drell-Yan Q_T distributions*, *Phys. Rev. D* **63** (2001) 114011, [hep-ph/0012348].
- [55] S. Catani, M. L. Mangano, P. Nason and L. Trentadue, *The Resummation of soft gluons in hadronic collisions*, *Nucl. Phys. B* **478** (1996) 273–310, [hep-ph/9604351].
- [56] E. Laenen, G. F. Sterman and W. Vogelsang, *Higher order QCD corrections in prompt photon production*, *Phys. Rev. Lett.* **84** (2000) 4296–4299, [hep-ph/0002078].

- [57] G. Lusterians, J. K. L. Michel, F. J. Tackmann and W. J. Waalewijn, *Joint two-dimensional resummation in q_T and 0-jettiness at NNLL*, *JHEP* **03** (2019) 124, [1901.03331].
- [58] A. Kulesza, G. F. Sterman and W. Vogelsang, *Joint resummation in electroweak boson production*, *Phys. Rev. D* **66** (2002) 014011, [hep-ph/0202251].
- [59] A. Kulesza, G. F. Sterman and W. Vogelsang, *Joint resummation for Higgs production*, *Phys. Rev. D* **69** (2004) 014012, [hep-ph/0309264].
- [60] J. Collins and T. Rogers, *Understanding the large-distance behavior of transverse-momentum-dependent parton densities and the Collins-Soper evolution kernel*, *Phys. Rev. D* **91** (2015) 074020, [1412.3820].
- [61] ATLAS collaboration, G. Aad et al., *A precise determination of the strong-coupling constant from the recoil of Z bosons with the ATLAS experiment at $\sqrt{s} = 8$ TeV*, 2309.12986.
- [62] V. Moos, I. Scimemi, A. Vladimirov and P. Zurita, *Extraction of unpolarized transverse momentum distributions from the fit of Drell-Yan data at N^4LL* , *JHEP* **05** (2024) 036, [2305.07473].
- [63] J. Collins, *Foundations of Perturbative QCD*, vol. 32. Cambridge University Press, 2011, 10.1017/9781009401845.
- [64] J. McGowan, T. Cridge, L. A. Harland-Lang and R. S. Thorne, *Approximate N^3LO parton distribution functions with theoretical uncertainties: MSHT20a N^3LO PDFs*, *Eur. Phys. J. C* **83** (2023) 185, [2207.04739].
- [65] G. Moreno et al., *Dimuon Production in Proton - Copper Collisions at $\sqrt{s} = 38.8$ -GeV*, *Phys. Rev. D* **43** (1991) 2815–2836.
- [66] A. S. Ito et al., *Measurement of the Continuum of Dimuons Produced in High-Energy Proton - Nucleus Collisions*, *Phys. Rev. D* **23** (1981) 604–633.
- [67] CDF collaboration, T. Aaltonen et al., *Transverse momentum cross section of e^+e^- pairs in the Z-boson region from $p\bar{p}$ collisions at $\sqrt{s} = 1.96$ TeV*, *Phys. Rev. D* **86** (2012) 052010, [1207.7138].
- [68] ATLAS collaboration, G. Aad et al., *A precise measurement of the Z-boson double-differential transverse momentum and rapidity distributions in the full phase space of the decay leptons with the ATLAS experiment at $\sqrt{s} = 8$ TeV*, *Eur. Phys. J. C* **84** (2024) 315, [2309.09318].
- [69] S. Alekhin et al., *HERAFitter*, *Eur. Phys. J. C* **75** (2015) 304, [1410.4412].
- [70] NNPDF collaboration, R. D. Ball et al., *The path to N^3LO parton distributions*, *Eur. Phys. J. C* **84** (2024) 659, [2402.18635].

- [71] MAP (MULTI-DIMENSIONAL ANALYSES OF PARTONIC DISTRIBUTIONS) collaboration, A. Bacchetta, V. Bertone, C. Bissolotti, G. Bozzi, M. Cerutti, F. Piacenza et al., *Unpolarized transverse momentum distributions from a global fit of Drell-Yan and semi-inclusive deep-inelastic scattering data*, *JHEP* **10** (2022) 127, [2206.07598].
- [72] M. G. Echevarria, A. Idilbi and I. Scimemi, *Factorization Theorem For Drell-Yan At Low q_T And Transverse Momentum Distributions On-The-Light-Cone*, *JHEP* **07** (2012) 002, [1111.4996].
- [73] LATTICE PARTON (LPC) collaboration, M.-H. Chu et al., *Lattice calculation of the intrinsic soft function and the Collins-Soper kernel*, *JHEP* **08** (2023) 172, [2306.06488].
- [74] A. Avkhadiev, P. E. Shanahan, M. L. Wagman and Y. Zhao, *Collins-Soper kernel from lattice QCD at the physical pion mass*, *Phys. Rev. D* **108** (2023) 114505, [2307.12359].
- [75] A. Avkhadiev, P. E. Shanahan, M. L. Wagman and Y. Zhao, *Determination of the Collins-Soper Kernel from Lattice QCD*, *Phys. Rev. Lett.* **132** (2024) 231901, [2402.06725].
- [76] D. Bollweg, X. Gao, S. Mukherjee and Y. Zhao, *Nonperturbative Collins-Soper kernel from chiral quarks with physical masses*, *Phys. Lett. B* **852** (2024) 138617, [2403.00664].
- [77] D. Bollweg, X. Gao, J. He, S. Mukherjee and Y. Zhao, *Transverse-momentum-dependent pion structures from lattice QCD: Collins-Soper kernel, soft factor, TMDWF, and TMDPDF*, *Phys. Rev. D* **112** (2025) 034501, [2504.04625].
- [78] LATTICE PARTON (LPC) collaboration, M.-H. Chu et al., *Nonperturbative determination of the Collins-Soper kernel from quasitransverse-momentum-dependent wave functions*, *Phys. Rev. D* **106** (2022) 034509, [2204.00200].
- [79] F. Aslan, M. Boglione, J. O. Gonzalez-Hernandez, T. Rainaldi, T. C. Rogers and A. Simonelli, *Phenomenology of TMD parton distributions in Drell-Yan and $Z0$ boson production in a hadron structure oriented approach*, *Phys. Rev. D* **110** (2024) 074016, [2401.14266].
- [80] A. B. Cuerpo, I. Scimemi and A. Vladimirov, *Assessing the sensitivity of Energy-Energy Correlations in e^+e^- annihilation to TMD dynamics*, 2507.17478.